International Journal of Computational Methods
(2025) 2441008 (16 pages)

DOI: 10.1142/S0219876224410081

Acoustic Characteristics of Laminar–Turbulent Transition in a Flat Plate Based on PSE and FW–H

Bohan Xie, Yuan Zhuang and Decheng Wan*
Computational Marine Hydrodynamic Lab (CMHL)
School of Naval Architecture, Ocean and Civil Engineering
Shanghai Jiao Tong University, Shanghai, P. R. China
**dcwan@sjtu.edu.cn*

Received 31 October 2024
Accepted 27 March 2025
Published 3 May 2025

In this study, nonlinear parabolized stability equation (PSE) and wall-resolved large-eddy simulation (WRLES) are employed to simulate laminar–turbulent transition in a flat plate using the solver OpenFOAM. Fluctuations of boundary layer displacement thickness, pressure and velocity in laminar, transition and turbulence regions are compared in detail. By combining nonlinear PSE and porous-surface Ffowcs-Williams and Hawkings (FW–H) method, the acoustic characteristics in different regions of the flat plate are analyzed. Our results have shown that the fluctuations of boundary layer displacement thickness and pressure in the transition region begin to increase. Besides, the fundamental wave and subharmonic wave introduced at the inlet boundary have a significant influence on the spectral curves of flow field quantities and radiated noise.

Keywords: Laminar–turbulent transition; parabolized stability equation; large-eddy simulation; radiated noise.

1. Introduction

Laminar–turbulent transition in a boundary layer has been extensively studied in recent decades. Laminar–turbulent transition occurs when an ambient disturbance enters the boundary layer and excites unstable disturbance waves, and the boundary layer eventually breaks into turbulence with the nonlinear interactions of disturbance waves [Erhard *et al.* (2010)]. The flow in the transition region is significantly different from that in the laminar region and turbulent region. It has been shown that the resistance of vehicles and the operation efficiency of propulsion systems are closely related to the transition onset position and transition region length [Narasimha (1985)]. However, the relevant research on the characteristics of radiated noise in transition regions is still scarce.

*Corresponding author.

Several numerical approaches have been developed to simulate laminar–turbulent transition process. Direct numerical simulation (DNS) has the highest accuracy in resolving small-magnitude disturbances in the boundary layer. By introducing a pair of oblique waves at low amplitudes in a supersonic flat-plate boundary layer, Mayer *et al.* [2011] demonstrated that oblique breakdown was a viable path to sustained turbulence. Subbareddy and Candler [2012] discussed the development of mean profiles in the transitional and fully turbulent regions by DNS and pointed out a “two-layer” structure in transitional regions. Sayadi *et al.* [2013] simulated complete transition to turbulence of both H-type and K-type, and discussed in detail the differences between the two types of transition. Drikakis *et al.* [2021] compared the transition acoustic loading at Mach 6 of DNS and implicit LES, it was found that DNS had advantages in predicting transition onset positions and high-frequency peaks.

Due to the high computational cost of DNS, linear stability theory (LST) is an alternative to simulating laminar–turbulent transition [Mack (1984)]. LST can be used to describe the linear growth of unstable modes. Jee *et al.* [2018] captured H-type breakdown generated by nonlinear interactions between the fundamental wave and the subharmonic oblique wave by LST. Danvin *et al.* [2018] demonstrated the performances of using LST in predicting the evolution of Mack’s second mode for compressible hypersonic flows. Bae *et al.* [2023] obtained rich high-fidelity computations by combining DNS and LST, and revealed that high spanwise wavenumber modes were associated with the final breakdown of the turbulent flow.

However, LST ignores the nonlocal and nonparallel effects in the boundary layer and thus is not suitable for simulating the nonlinear growth of the disturbances. Parabolized stability equation (PSE) proposed by Herbert [1997] well solved the problem, and was capable of simulating laminar–turbulent transition economically. Lozano *et al.* [2018] reproduced downstream turbulence by modeling pretransitional regions with PSE. Kim *et al.* [2019] managed to reproduce the subharmonic resonance by nonlinear PSE, and pointed out that the PSE inlet located downstream could effectively reduce computational cost. Based on PSE, Olichevis *et al.* [2021] proposed a robust transition framework to conduct PSE calculations for transition onset locations.

In this paper, wall-resolved large-eddy simulation (WRLES) and nonlinear PSE are adopted to simulate laminar–turbulent transition in a flat plate. The evolutions of the flow field in the laminar, transition and turbulence regions are analyzed. Furthermore, the acoustic characteristics in different regions are evaluated by Ffowcs-Williams and Hawkings (FW–H) method.

2. Numerical Methods

2.1. *Large-eddy simulation*

LES separates large-scale and small-scale eddies in the flow field by filtering functions. Large-scale eddies are directly simulated, and small-scale eddies are resolved by sub-grid scale models [Smagorinsky (1963)]. The spatially filtered governing equations are expressed as follows:

$$\frac{\partial \bar{u}_i}{\partial x_i} = 0, \tag{1}$$

$$\frac{\partial \bar{u}_i}{\partial t} + \frac{\partial}{\partial x_j}(\bar{u}_i \bar{u}_j) = -\frac{1}{\rho}\frac{\partial \bar{p}}{\partial x_i} + \nu \frac{\partial^2 \bar{u}_i}{\partial {x_j}^2} - \frac{\partial \tau_{ij}}{\partial x_j}, \tag{2}$$

where the subscripts i and j represent streamwise, normal and spanwise directions, the symbol $\bar{\cdot}$ denotes the spatial filtering, p is the pressure, ν is the kinematic viscosity of fluid and $\tau_{ij} = \bar{u}_i \bar{u}_j - \overline{u_i u_j}$ is the sub-grid stress to describe the interactions between the large-scale eddies and small-scale eddies.

The wall-adapting local eddy-viscosity (WALE) model is adopted in this study. WALE is a sub-grid scale model based on the square of the velocity gradient tensor, which takes both the shear stress tensor and the rotation tensor into account [Nicoud and Ducros (1999)]. The expression of sub-grid viscosity ν_t of WALE is as follows:

$$\nu_t = (C_w \Delta)^2 \frac{(S_{ij}^d S_{ij}^d)^{3/2}}{(\bar{S}_{ij}\bar{S}_{ij})^{5/2} + (S_{ij}^d S_{ij}^d)^{5/4}}, \tag{3}$$

where C_w is the model coefficient, Δ is the grid filter width defined by cell volume and S_{ij}^d is the tensor defined as follows:

$$S_{ij}^d = \frac{1}{2}\left(\frac{\partial \bar{u}_i}{\partial x_k}\frac{\partial \bar{u}_k}{\partial x_j} + \frac{\partial \bar{u}_j}{\partial x_k}\frac{\partial \bar{u}_k}{\partial x_i}\right) - \frac{1}{3}\delta_{ij}\frac{\partial \bar{u}_k}{\partial x_k}\frac{\partial \bar{u}_k}{\partial x_k}. \tag{4}$$

2.2. *Parabolized stability equation*

The variables $\check{\phi}$ in the flow field can be decomposed into the following form:

$$\check{\phi} = \Phi + \phi, \tag{5}$$

where Φ is the mean quantity and ϕ is the disturbance.

The basic idea of PSE is to decompose each mode in a disturbance ϕ into a slow-varying shape function and a fast-varying wave function [Herbert and Bertolotti (1987)]. Assuming that the disturbance ϕ is periodic in both spanwise and time, it can be expressed in the following Fourier series form:

$$\begin{aligned} \phi(x,y,z,t) = &\sum_{m=-N_m}^{N_m}\sum_{n=-N_n}^{N_n} \hat{\phi}_{(m,n)}(x,y) \\ &\times \left[\exp i \int_{x0}^{x} \alpha_{(m,n)}(\xi)d\xi + in\beta z - im\omega t\right], \end{aligned} \tag{6}$$

where x, y, z indicate streamwise, normal and spanwise directions, respectively, $\hat{\phi}_{(m,n)}$ is the shape function of Fourier mode (m,n), $\alpha_{(m,n)}$ is the streamwise complex wave number of Fourier mode (m,n), subscripts m and n are the temporal and spanwise wave modes, respectively, β is the spanwise wave number and ω is the angular frequency.

In this study, nonlinear PSE is used to calculate nonlinear growth of disturbances at the early stage, and the downstream nonlinear interactions and transition to the turbulence are simulated by LES instead.

2.3. *Ffowcs-Williams and Hawking's equation*

Noise generated by fluid was first equivalent to sound sources by the acoustic analogy proposed by Lighthill [1952]. Based on Lighthill's theory, Ffowcs-Williams and Hawkings [1969] derived the FW–H equation, which extended Lighthill's theory to the case of considering a rigid boundary with arbitrary motion in the flow field. The original FW–H equation is shown as follows:

$$\odot^2 p' = \frac{\partial}{\partial t}[\rho_0 v_n \delta(f)] - \frac{\partial}{\partial x_i}[p n_i \delta(f)] + \frac{\partial^2}{\partial x_i \partial x_j}[H(f) T_{ij}], \tag{7}$$

$$T_{ij} = \rho u_i u_j - \sigma_{ij} + (p' - c^2 \rho')\delta_{ij}, \tag{8}$$

where $\odot^2 = \frac{1}{c^2}\frac{\partial^2}{\partial t^2} - \nabla^2$ is the D'Alembert operator, $\rho' = \rho - \rho_0$ is the density perturbation, c is the velocity of sound in the fluid, ρ_0 is the density of the fluid, v_n is the normal velocity of the integral surface, T_{ij} is the Lighthill's stress tensor, σ_{ij} is the viscous stress tensor, δ_{ij} is the Kronecker symbol, $\delta(f)$ is the Dirac function and $H(f)$ is the Heaviside function.

In this study, the porous-surface FW–H method proposed by Di Francescantonio [1997] is applied rather than the original one. The reason will be mentioned later. The porous-surface FW–H equation can be expressed as

$$\odot^2 p' = \frac{\partial}{\partial t}[\rho_0 U_n \delta(f)] - \frac{\partial}{\partial x_i}[L_i \delta(f)] + \frac{\partial^2}{\partial x_i \partial x_j}[H(f) T_{ij}], \tag{9}$$

$$U_n = \left(1 - \frac{\rho}{\rho_0}\right) v_n + \frac{\rho u_n}{\rho_0}, \tag{10}$$

$$L_i = p\delta_{ij} n_j + \rho u_i (u_n - v_n). \tag{11}$$

Farassat's formulation 1A converted the FW–H equation into integral form as follows [Brentner and Farassat (1998)]:

$$p'_S(x,t) = p'_T(x,t) + p'_L(x,t), \tag{12}$$

$$4\pi p'_T(x,t) = \int_{f=0} \left[\frac{\rho_0 \dot{v_n}}{r(1-Mr)^2} + \frac{\rho_0 v_n \hat{r_i} \dot{M_i}}{r(1-Mr)^3}\right]_{\text{ret}} dS + \int_{f=0} \left[\frac{\rho_0 c v_n \left(M_r - M^2\right)}{r^2 (1-Mr)^3}\right]_{\text{ret}} dS, \tag{13}$$

$$4\pi p'_L(x,t) = \int_{f=0} \left[\frac{\dot{p}\cos\theta}{cr(1-Mr)^2} + \frac{\hat{r}_i \dot{M}_i p\cos\theta}{cr(1-Mr)^3} \right]_{\text{ret}} dS + \int_{f=0} \left[\frac{p(\cos\theta - M_i n_i)}{r^2(1-Mr)^2} + \frac{(M_r - M^2)p\cos\theta}{r^2(1-Mr)^3} \right]_{\text{ret}} dS, \quad (14)$$

where $p'_S(x,t)$ is the total surface term, $p'_T(x,t)$ is the thickness surface term, $p'_L(x,t)$ is the loading surface term, $1 - Mr$ is the Doppler factor, $r = |x - y|$ is the distance from the sound source to the observer, subscript ret represents the retarded time $t - r/c$.

The sound pressure level (SPL) is defined as

$$\text{SPL} = 20\log_{10}(p/p_{\text{ref}}), \quad (15)$$

where p is the acoustic pressure fluctuations and $p_{\text{ref}} = 1\,\mu\text{Pa}$ is the reference pressure for water. To represent the total level of SPL in a specific frequency band, the overall sound pressure level (OASPL) is defined as

$$\text{OASPL} = 20\log_{10}\left(\sum_{i=1}^{N} 10^{\text{SPL}_i/10}\right), \quad (16)$$

where SPL_i is the SPL value corresponding to the frequency i and N is the number of frequency points in the frequency band.

The current FW–H code in OpenFOAM refers to Epikhin *et al.* [2015].

2.4. *Numerical setup*

In this paper, LES coupled with nonlinear PSE is used to simulate the laminar–turbulent transition in a flat plate. The current computational domain is shown in Fig. 1, where $R = \sqrt{\text{Re}_x} = \sqrt{\frac{U_\infty x}{\nu}}$ denotes the nondimensional streamwise position. The freestream velocity $U_\infty = 1\,\text{m/s}$ and the kinematic viscosity of the fluid $\nu = 6.25 \times 10^{-6}\,\text{m}^2/\text{s}$. The upstream laminar simulation is conducted between $0 \le R < 400$, where $R = 400$ is the outlet for the laminar region as well as the inlet for the turbulence region. Flow field information of both laminar simulation and nonlinear PSE calculation are input at $R = 400$. Laminar–turbulent transition and full turbulence are resolved at the turbulence region between $400 \le R < 1000$. The sponge region with $1000 \le R \le 1300$ is set to reduce the influence of the outlet boundary on the flow. The boundary layer thickness $\delta_0 = 0.01\,\text{m}$ at $R = 400$ is used to nondimensionalize the length scale. The length, height and width of the computational domain are $L_x = 1050\delta_0$, $L_y = 300\delta_0$ and $L_z = 12\delta_0$, respectively.

According to Kachanov's experiment [Kachanov and Levchenko (1984)], a fundamental wave with mode $(2,0)$ of $F = 2\pi f\nu/U_\infty^2 = 124 \times 10^{-6}$ ($f\delta_0/U_\infty = 3.2 \times 10^{-2}$), and a pair of subharmonic wave with mode $(1,1)$ of $\frac{1}{2}F$ ($f\delta_0/2U_\infty = 1.6 \times 10^{-2}$) are introduced at $R = 400$. The streamwise wave number of the 2D Tollmien–Schlichting (TS) wave is $\alpha_{(2,0)} = 2\pi\delta_0/\lambda_x = 0.5418$, the spanwise

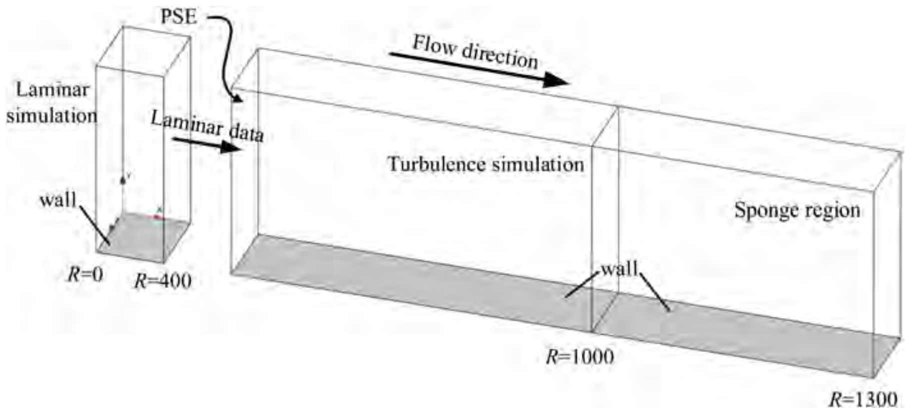

Fig. 1. Computational domain.

Table 1. Grid parameters.

Parameters	Laminar simulation	Turbulence simulation	Sponge region
Δx^+	9.62	9.21	901.20
$\Delta y^+_{\min}$	0.75	0.81	0.53
$\Delta y^+_{\max}$	767.92	824.98	536.15
Δz^+	9.07	9.78	6.35
N_x	500	3000	60
N_y	128	128	128
N_z	64	64	64
$N_{\text{total}} \times 10^6$	4.096	24.576	0.492

wavenumber of the subharmonic wave is $\beta_{(1,1)} = 2\pi\delta_0/\lambda_z = 0.5206$, and the angular frequency of the TS wave is $\omega_{(2,0)} = 2\pi f \delta_0/U_\infty = 0.1984$.

Hexahedral grids with a total number of 2.916×10^7 are employed for the current simulation. The streamwise and spanwise scales of grids are isotropic. The normal scale of grids increases gradually as the distance to the boundary increases. Detailed grid parameters are shown in Table 1. The superscript + represents nondimensional by friction velocity u_τ and viscosity ν. The timestep used in the current simulation is $\Delta t_1 U_\infty/\delta_0 = 0.1$ for over $T_1 U_\infty/\delta_0 = 4000$ to obtain a steady flow, and is adjusted to $\Delta t_2 U_\infty/\delta_0 = 0.005$ for over $T_2 U_\infty/\delta_0 = 500$ to record unsteady flow information like pulsating pressure and noise.

3. Numerical Simulations

The instantaneous vortex structure displayed based on the Q-criterion [Hunt *et al.* (1988)] is shown in Fig. 2. At the upstream region, the 2D TS wave is the dominant component. As the flow moves downstream, the amplitude of the subharmonic wave

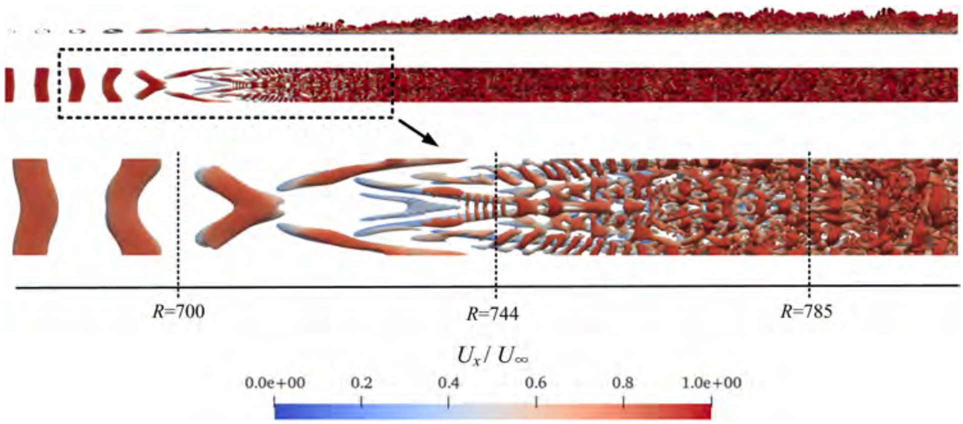

Fig. 2. Isosurface of $Q = 5\,\mathrm{s}^{-2}$ colored by nondimensional streamwise velocity.

gradually increases to the same order as the fundamental wave, leading to spanwise fluctuations in the flow field. The three-dimensional instability promotes the evolution and interaction of vortex structures. As a consequence, turbulent spots and gamma vortex appear, which marks the beginning of the transition to turbulence. Turbulence spots continue to grow and develop downstream and merge with other turbulence spots, and eventually forming a fully developed turbulent flow [Emmons (1951)].

The skin friction coefficient C_f, defined as $C_f = \frac{\tau_w}{\frac{1}{2}\rho U_\infty^2}$, where τ_w is the mean wall shear stress, is an important parameter to describe the transition from laminar to turbulence. The streamwise distribution C_f of the current simulation compared with previous studies is shown in Fig. 3 [Sayadi *et al.* (2013); Lozano *et al.* (2018); Kim *et al.* (2019)]. The evolution of C_f shows that PSE coupled with the LES method is able to resolve laminar–turbulent transition process accurately. It is generally believed that the location where C_f curve derivates from the laminar solution represents the onset of transition, and the transition ends at the peak of C_f curve. According to the current results, $R = 700$ and $R = 785$ are used to represent the onset and end of laminar–turbulent transition, respectively. Thus, the length of the transition region is $\Delta x_{\mathrm{tr}} = 79\delta_0$.

Three FW–H porous surfaces are employed to predict the radiated noise level in laminar, transition and turbulence regions, as shown in Fig. 4. All FW–H sound source regions are $79\delta_0$ in length, $30\delta_0$ in height and $30\delta_0$ in width, to ensure that each sound source region has the same resolution and number of grid cells. Three observers (M1, M2, M3) are located $100\delta_0$ from the wall, and at the center of each FW–H sound source region in streamwise and spanwise directions, respectively. Each observer only corresponds to the FW–H porous surface directly below to avoid the influence of the sound propagation distance. An additional observer N1 located $1000\delta_0$ from the onset of transition corresponds to the porous surface at the

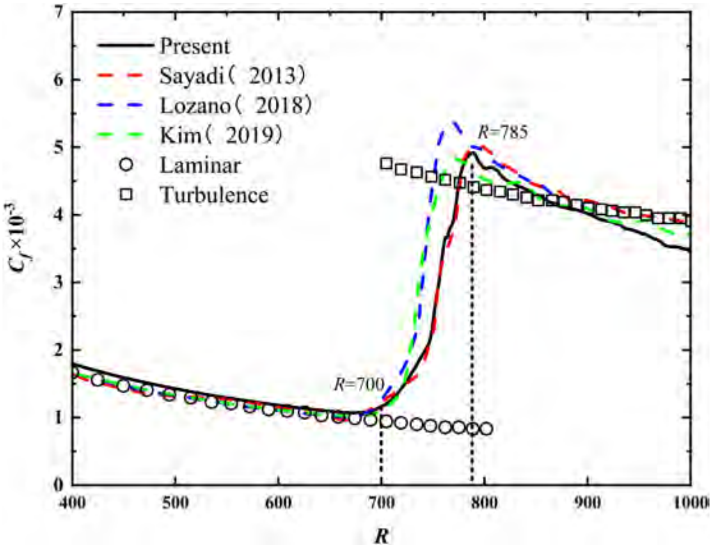

Fig. 3. Streamwise distribution of C_f in the flat plate.

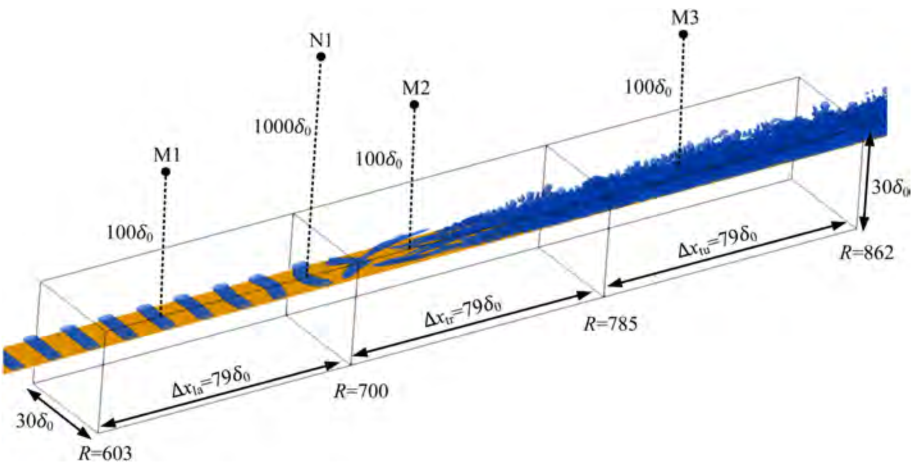

Fig. 4. Schematic diagram of the radiated noise prediction.

transition region and is used to verify the simulation results of radiated noise in the transition region in a flat plate.

Lauchle [1981] derived the empirical formula for the power spectral density (PSD) of the far-field acoustic pressure radiated per unit spanwise width of the boundary layer in the transition region of a flat plate by equating the displacement thickness fluctuation to a monopole sound source. The FW–H method based on the stationary surface cannot take monopole noise into account, so it is not suitable

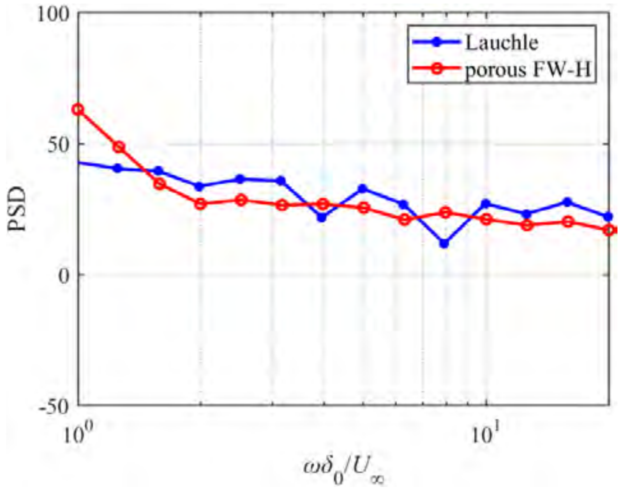

Fig. 5. Comparison of PSD between Lauchle's empirical formula and current porous FW–H method in the transition region on the plate.

for predicting the radiated noise in the transition region. The comparison between the current porous FW–H method and Lauchle's empirical formula at observer N1 is shown in Fig. 5, where ω is normalized by δ_0 and U_∞. Considering that the empirical formula is idealized in some aspects, the present comparative results are generally in good agreement. This proves that the porous FW–H method is able to accurately predict the radiated noise in the transition region.

To further study the radiated noise characteristics on the flat plate, Fig. 6 provides comparisons of SPL in laminar, transition and turbulence regions. In Fig. 6(a), one-third octave spectral of SPL from $0.1 < \omega\delta_0/U_\infty < 20$ indicate that noise

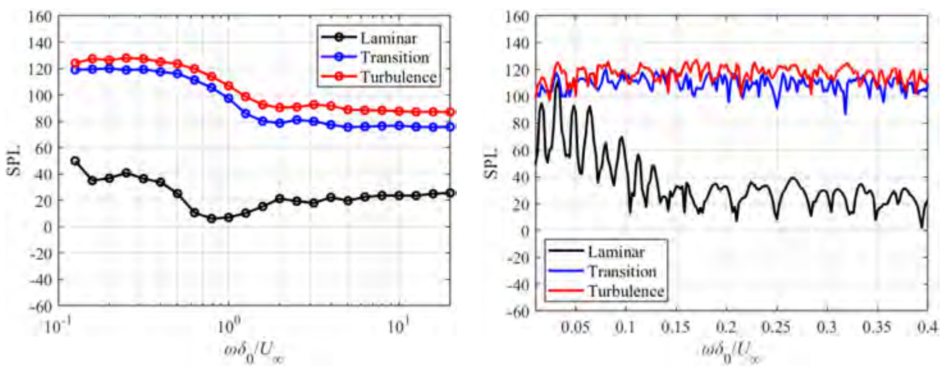

Fig. 6. Comparisons of SPL in different regions on the plate. (a) One-third octave spectral and (b) Continuous spectral.

generated in the laminar region is much lower than that in the transition region and turbulence region in each frequency band. SPL curves in the transition region and turbulence region have similar frequency variation regulation, and noise in the turbulence region is slightly greater than that in the transition region. Since the high SPL amplitude parts in each region are concentrated in the low-frequency segment, Fig. 6(b) compares the continuous spectral of SPL from $0.01 < \omega\delta_0/U_\infty < 0.4$ in different regions. The low-frequency noise of the transition region and turbulence region is almost of similar magnitude without obvious SPL peaks. However, the extremely low frequency ($\omega\delta_0/U_\infty < 0.128$) noise in the laminar region exhibits significant spectral line characteristics with $\Delta\omega\delta_0/U_\infty = 1.6\times10^{-2}$, which is very close to the frequency of subharmonic wave introduced at the inlet. When the $\omega\delta_0/U_\infty$ is higher than 0.16, the frequency interval of adjacent SPL peaks is approximately doubled in the laminar region. This phenomenon seems to suggest that the frequency features of radiated noise in the laminar region are significantly affected by TS wave and subharmonic wave. Flows in transition and turbulent regions are more intense, resulting in more complex sound sources of radiated noise. Therefore, the frequencies corresponding to the TS wave and subharmonic wave are no longer dominant in radiated noise.

In order to explore the relationship between flow field characteristics and radiated noise in different regions of the flat plate, the different regions of the flat plate are divided into four parts with equal area, as shown in Fig. 7. The changes of pulsating pressure, velocity and boundary layer displacement thickness δ^* are analyzed at the positions marked in the figure. δ^* is defined as follows:

$$\delta^* = \int_0^\delta \left(1 - \frac{u}{U_\infty}\right) dy, \tag{17}$$

where u is the local streamwise velocity, δ is the boundary layer thickness defined as the distance from the boundary where u reaches 99% of U_∞.

Comparisons of PSD of boundary layer displacement thickness δ^* are shown in Fig. 8. The PSD results are nondimensionalized by δ_0 and f, where f is the frequency of fundamental wave satisfying $f\delta_0/U_\infty = 3.2\times10^{-2}$. Both in the laminar region and turbulence region, the PSD of δ^* hardly changes in different streamwise locations. In the transition region, the PSD value increases significantly with the increase of R in the frequency band $\omega\delta_0/U_\infty > 0.04$. For all the typical locations, PSD curves reach peaks around $\omega\delta_0/U_\infty = 1.6 \times 10^{-2}$ and $\omega\delta_0/U_\infty = 3.2 \times 10^{-2}$. These results indicate that the fluctuations of boundary layer displacement thickness in the

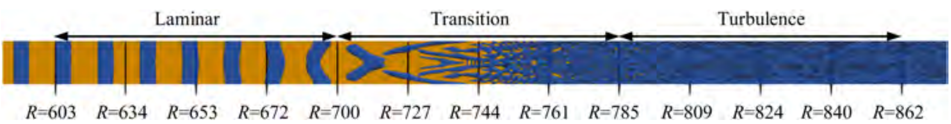

Fig. 7. Typical locations of different regions on the plate.

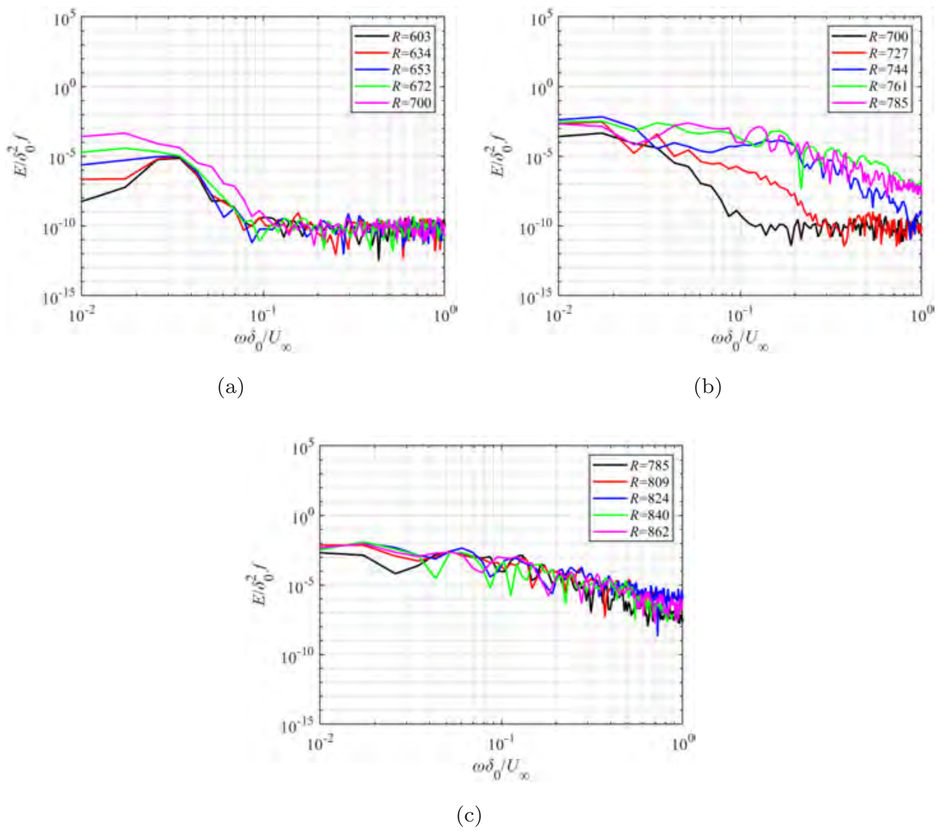

Fig. 8. PSD of boundary layer displacement thickness δ^* in different regions on the plate. (a) Laminar region, (b) Transition region and (c) Turbulence region.

transition region begin to intensify, which confirms Lauchle's hypothesis [Lauchle (1981)]. In addition, the TS wave and subharmonic wave introduced at the inlet boundary could affect fluctuations in the boundary layer displacement thickness.

Pressure and normal velocity are monitored in the typical streamwise locations in Fig. 7 at $y = 0.1\delta_0$ (in the near-wall region) and $y = 10\delta_0$ (at the porous FW–H surface, in the freestream). Comparisons of SPL curves of pressure nondimensionalized by $p_{\text{ref}} = 1\,\mu\text{Pa}$ are shown in Fig. 9. In the laminar region and early transition region at $y = 0.1\delta_0$, several peaks in SPL curves with the frequency interval of $\Delta\omega\delta_0/U_\infty = 1.6 \times 10^{-2}$ are observed at low frequency. At the downstream locations, the pulsating pressure has a higher order of magnitude throughout the low frequency. Besides, the pulsating pressure gradually increases from the onset of transition the full turbulence is developed. These phenomena indicate that the instability modes imposed by nonlinear PSE have an influence on the pre-transition and early-transition regions. However, it seems that these subharmonic and higher harmonic waves only affect the pulsating pressure in the near-wall region, due to

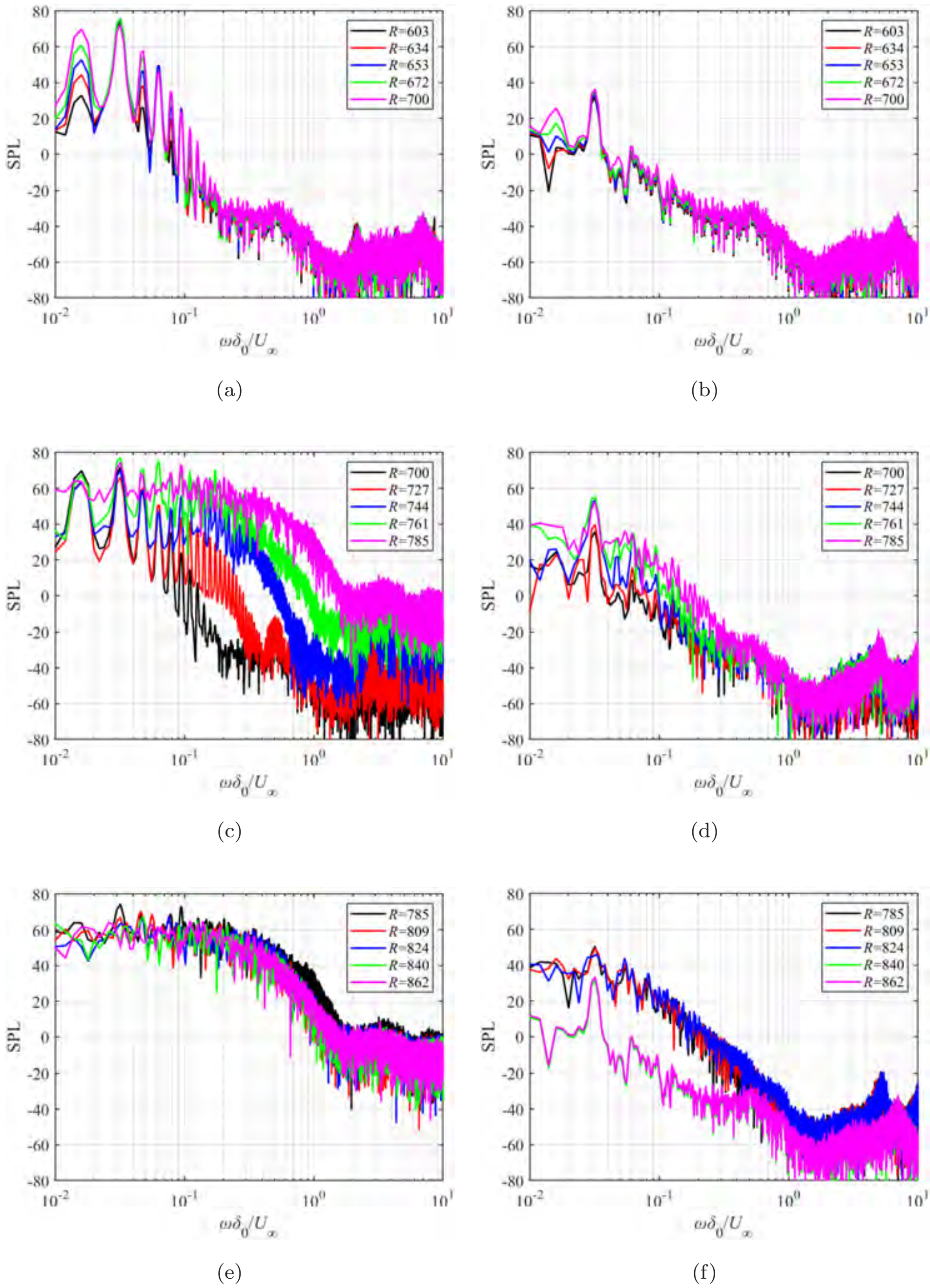

Fig. 9. SPL of pressure in different regions on the plate. (a) $y = 0.1\delta_0$ in laminar region, (b) $y = 10\delta_0$ in laminar region, (c) $y = 0.1\delta_0$ in transition region, (d) $y = 10\delta_0$ in transition region, (e) $y = 0.1\delta_0$ in turbulence region and (f) $y = 10\delta_0$ in turbulence region.

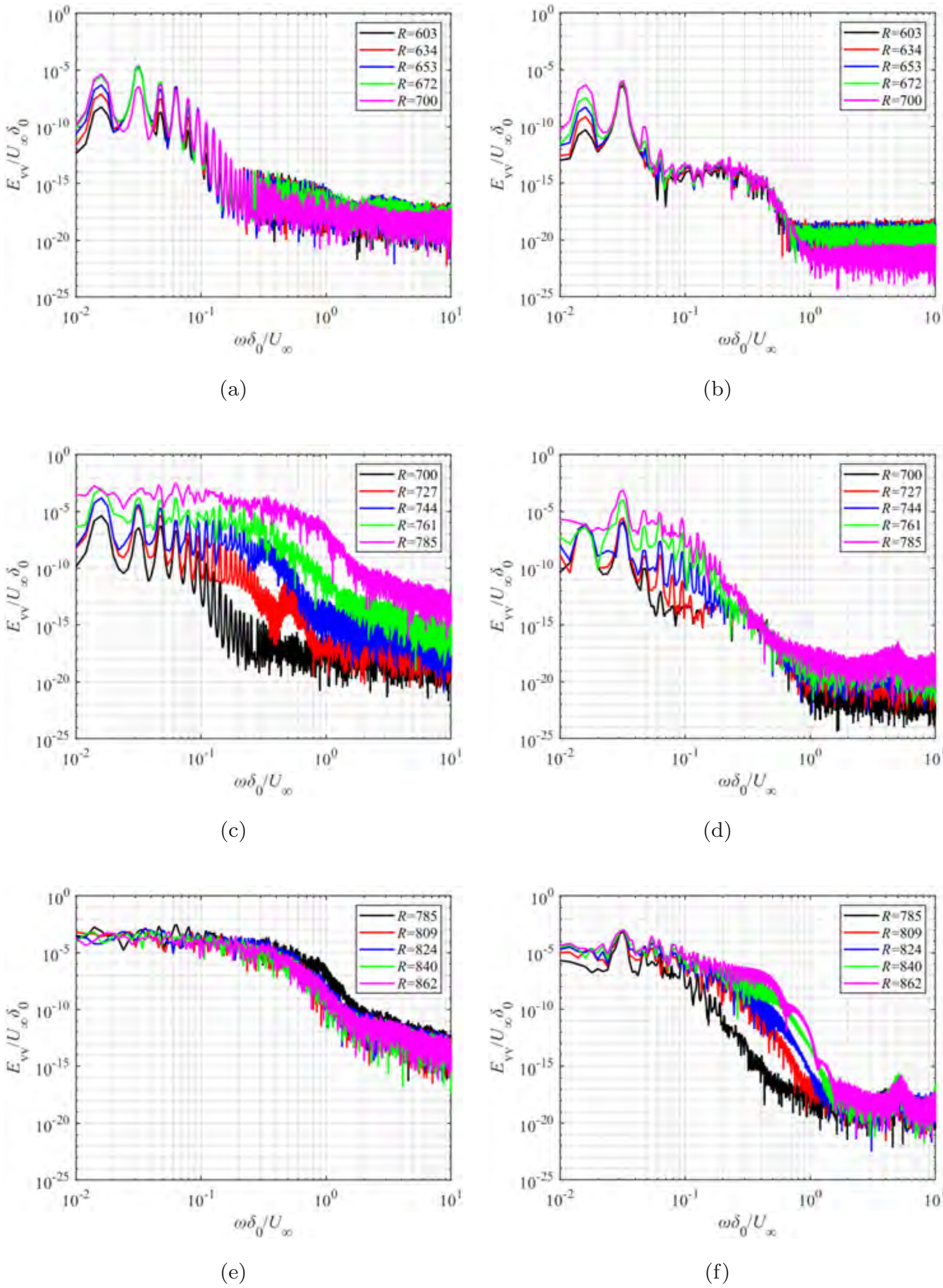

Fig. 10. PSD of normal velocity in different regions on the plate. (a) $y = 0.1\delta_0$ in laminar region, (b) $y = 10\delta_0$ in laminar region, (c) $y = 0.1\delta_0$ in transition region, (d) $y = 10\delta_0$ in transition region, (e) $y = 0.1\delta_0$ in turbulence region and (f) y=$10\delta_0$ in turbulence region.

only the peak of SPL curves corresponding to the frequency of the TS wave being detected in the freestream. According to the FW–H equation, the fluctuations of pressure can be regarded as a dipole sound source [Ffowcs-Williams and Hawkings (1969)]. The present numerical results show that this dipole sound source is mainly concentrated in the near-wall region, and is closely related to the disturbance modes.

The normal velocity at $y = 0.1\delta_0$ and $y = 10\delta_0$ represents the expansion of the boundary layer to the outside and the normal velocity through the porous FW–H surfaces, respectively. The PSD curves of normal velocity nondimensionalized by U_∞ and δ_0 in different regions are shown in Fig. 10. In the near-wall region, the PSD curves of normal velocity have a similar variation trend with SPL curves of pulsating pressure, including the frequency characteristics. This proves once again that the influence of the disturbed modes on the flow field is comprehensive. Fluctuations of normal velocity in the transition region gradually increase at $y = 0.1\delta_0$, which corresponds to the conclusion mentioned above that the fluctuations of the boundary layer displacement thickness intensify. The normal velocity at $y{=}10\delta_0$ represents the monopole sound source of the FW–H equation [Ffowcs-Williams and Hawkings (1969)]. Dominant peaks of PSD curves in different regions also occur at $\omega\delta_0/U_\infty = 3.2 \times 10^{-2}$. Unlike the results of pulsating pressure, the normal velocity still increases in further downstream locations in the turbulence region. Therefore, the monopole noise generated in the turbulent region is theoretically much greater than that in the laminar flow region and the transition region.

4. Conclusions

In this paper, WRLES coupled with nonlinear PSE and porous-surface FW–H method is applied in the current simulation to resolve the flow field and acoustic characteristics of the laminar–turbulent transition in a flat plate. Compared to the previous studies, our numerical results are convincing. The fluctuations of boundary layer displacement thickness, pressure, velocity and radiated noise in different regions of the flat plate are compared and analyzed. According to our simulation results, the disturbance modes imposed at the inlet boundary by PSE have a great influence on the fluctuations of pressure and normal velocity in the laminar region and early transition region. Spectral curves of these parameters have obvious peaks at the frequencies of the TS wave and subharmonic wave especially in the near-wall region. From the onset of transition, the fluctuations of pressure, normal velocity and boundary layer displacement thickness increase significantly with the increase of R. In the late-transition region and fully developed turbulence region, the flow becomes more complex and is no longer dominated by the disturbance modes. Therefore, spectral for the above flow field parameters and radiated noise show a high order at the low frequency in the both transition and turbulence regions without frequency peaks. Because the pulsating pressure and normal velocity gradually increase in the transition region, the radiated noise level in the transition region is slightly lower than that in the turbulence region.

Acknowledgment

This work is supported by the National Natural Science Foundation of China (52131102), to which the authors are most grateful.

ORCID

Bohan Xie https://orcid.org/0009-0000-8818-0760

Yuan Zhuang https://orcid.org/0009-0000-9183-5772

Decheng Wan https://orcid.org/0000-0002-1279-3891

References

Bae, H., Lim, J., Kim, M. and Jee, S. [2023] "Direct-numerical simulation with the stability theory for turbulent transition in hypersonic boundary layer," *Int. J. Aeronaut. Space Sci.* **24**(4), 1004–1014.

Brentner, K. S. and Farassat, F. [1998] "Analytical comparison of the acoustic analogy and Kirchhoff formulation for moving surfaces," *AIAA J.* **36**(8), 1379–1386.

Danvin, F., Olazabal-Loume, M. and Pinna, F. [2018] "Laminar to turbulent transition prediction in hypersonic flows with metamodels," in *Proc.* 2018 *Fluid Dynamics Conf.*, Atlanta, Georgia (American Institute of Aeronautics and Astronautics), pp. 1–18.

Di Francescantonio, P. [1997] "A new boundary integral formulation for the prediction of sound radiation," *J. Sound Vib.* **202**(4), 491–509.

Drikakis, D., Ritos, K., Spottswood, S. M. and Riley, Z. B. [2021] "Flow transition to turbulence and induced acoustics at Mach 6," *Phys. Fluids* **33**(7), 076112.

Emmons, H. W. [1951] "The laminar–turbulent transition in a boundary layer — Part I," *J. Aeronaut. Sci.* **18**(7), 490–498.

Epikhin, A., Evdokimov, I., Kraposhin, M., Kalugin, M. and Strijhak, S. [2015] "Development of a dynamic library for computational aeroacoustics applications using the OpenFOAM open source package," *Procedia Comput. Sci.* **66**, 150–157.

Erhard, P., Etling, D., Muller, U., Riedel, U. and Sreenivasan, K. R. [2010] *Prandtl-Essentials of Fluid Mechanics* (Springer Science & Business Media).

Ffowcs-Williams, J. E. and Hawkings, D. L. [1969] "Sound generation by turbulence and surfaces in arbitrary motion," *Philos. Trans. R. Soc. Lond. Ser. A Math. Phys. Sci.* **264**, 321–342.

Herbert, T. [1997] "Parabolized stability equations," *Annu. Rev. Fluid Mech.* **29**(1), 245–283.

Herbert, T. and Bertolotti, F. P. [1987] "Stability analysis of nonparallel boundary layers," *Bull. Am. Phys. Soc.* **32**(2079), 590.

Hunt, J. C. R., Wray, A. A. and Moin, P. [1988] "Eddies, streams, and convergence zones in turbulent flows," in *Studying Turbulence Using Numerical Simulation Databases*, 2. *Proc.* 1988 *Summer Program* (Center for Turbulence Research, NASA Ames/Stanford University), pp. 193–208.

Jee, S., Joo, J. and Lin, R. S. [2018] "Toward cost-effective boundary layer transition computations with large-eddy simulation," *J. Fluids Eng.* **140**(11), 111201.

Kachanov, Y. S. and Levchenko, V. Y. [1984] "The resonant interaction of disturbances at laminar–turbulent transition in a boundary layer," *J. Fluid Mech.* **138**, 209–247.

Kim, M., Lim, J., Kim, S., Jee, S., Park, J. and Park, D. [2019] "Large-eddy simulation with parabolized stability equations for turbulent transition using OpenFOAM," *Comput. Fluids* **189**, 108–117.

Lauchle, G. C. [1981] "Transition noise — The role of fluctuating displacement thickness," *J. Acoust. Soc. Am.* **69**(3), 665–671.

Lighthill, M. J. [1952] "On sound generated aerodynamically I. General theory," *Proc. R. Soc. Lond. Ser. A Math. Phys. Sci.* **211**(1107), 564–587.

Lozano, D. A., Hack, M. J. P. and Moin, P. [2018] "Modeling boundary-layer transition in direct and large-eddy simulations using parabolized stability equations," *Phys. Rev. Fluids* **3**(2), 023901.

Mack, L. M. [1984] Boundary-layer linear stability theory, AGARD Report No. **709**, Part 3, pp. 1–3.

Mayer, C. S. J., Von Terzi, D. A. and Fasel, H. F. [2011] "Direct numerical simulation of complete transition to turbulence via oblique breakdown at Mach 3," *J. Fluid Mech.* **674**, 5–42.

Narasimha, R. [1985] "The laminar–turbulent transition zone in the boundary layer," *Prog. Aerosp. Sci.* **22**(1), 29–80.

Nicoud, F. and Ducros, F. [1999] "Subgrid-scale stress modelling based on the square of the velocity gradient tensor," *Flow Turbul. Combust.* **62**(3), 183–200.

Olichevis, H. G. L., Fidkowski, K. J. and Martins, J. R. R. A. [2021] "Toward automatic parabolized stability equation-based transition-to-turbulence prediction for aerodynamic flows," *AIAA J.* **59**(2), 462–473.

Sayadi, T., Hamman, C. W. and Moin, P. [2013] "Direct numerical simulation of complete H-type and K-type transitions with implications for the dynamics of turbulent boundary layers," *J. Fluid Mech.* **724**, 480–509.

Smagorinsky, J. [1963] "General circulation experiments with the primitive equations: I. The basic experiment," *Mon. Weather Rev.* **91**(3), 99–164.

Subbareddy, P. and Candler, G. [2012] "DNS of transition to turbulence in a Mach 6 boundary layer," in *Proc. 43rd AIAA Thermophysics Conf.*, New Orleans, Louisiana (American Institute of Aeronautics and Astronautics), pp. 1–14.